

## Supplementary Information

### **Approaching the fill factor Shockley-Queisser limit in stable, dopant-free triple cation perovskite solar cells**

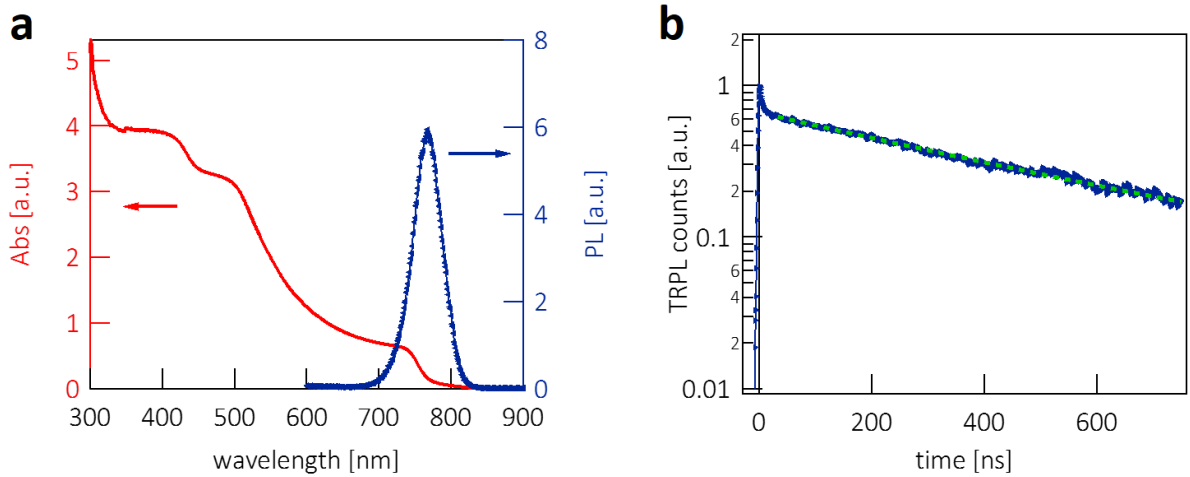
MARTIN STOLTERFOHT<sup>\*,<sup>◦</sup>,1</sup>, CHRISTIAN M. WOLFF<sup>◦,1</sup>, YOHAI AMIR<sup>1</sup>, ANDREAS PAULKE<sup>1</sup>,  
LORENA PERDIGÓN-TORO<sup>1</sup>, PIETRO CAPRIOGLIO<sup>1,2</sup>, DIETER NEHER<sup>\*,1</sup>

<sup>1</sup> *Institute of Physics and Astronomy, University of Potsdam, Karl-Liebknecht-Str. 24-25, D-14476 Potsdam-Golm, Germany.*

<sup>2</sup> *Institut für Silizium Photovoltaik, Helmholtz-Zentrum Berlin für Energie und Materialien, Kekuléstrasse 5, 12489 Berlin, Germany*

*E-mail:* [stolterf@uni-potsdam.de](mailto:stolterf@uni-potsdam.de), [neher@uni-potsdam.de](mailto:neher@uni-potsdam.de)

*(<sup>◦</sup> The first two authors contributed equally to this work.)*



**Supplementary Figure S1.** (a) Spectral absorption and photoluminescence of a triple cation perovskite film on glass. (b) The transient photoluminescence decay of a triple cation perovskite film on a glass substrate measured at 400 nm at a fluence of  $50 \text{ nJcm}^{-2}$  and a repetition rate of 500 kHz. The long time decay is nearly monoexponential and exhibits a lifetime of approximately 486 ns.

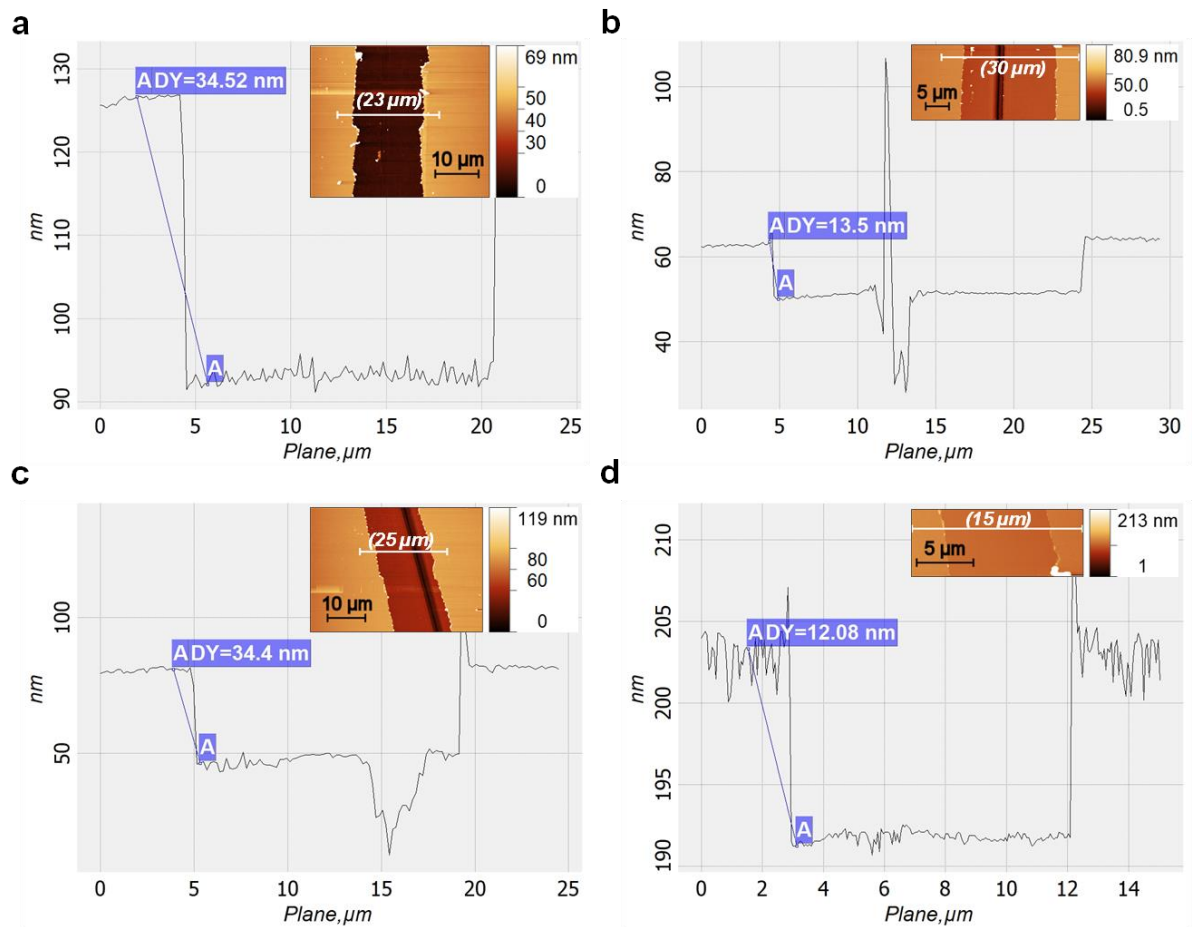
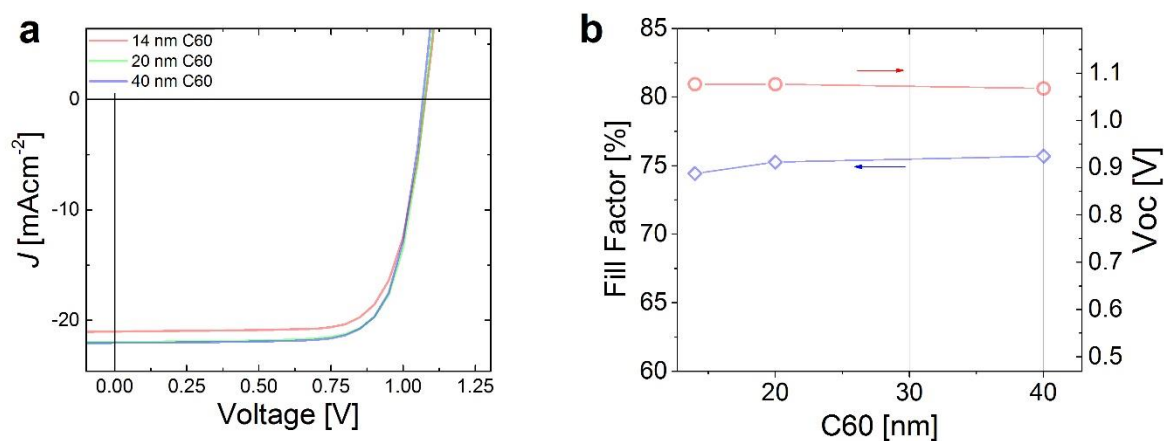
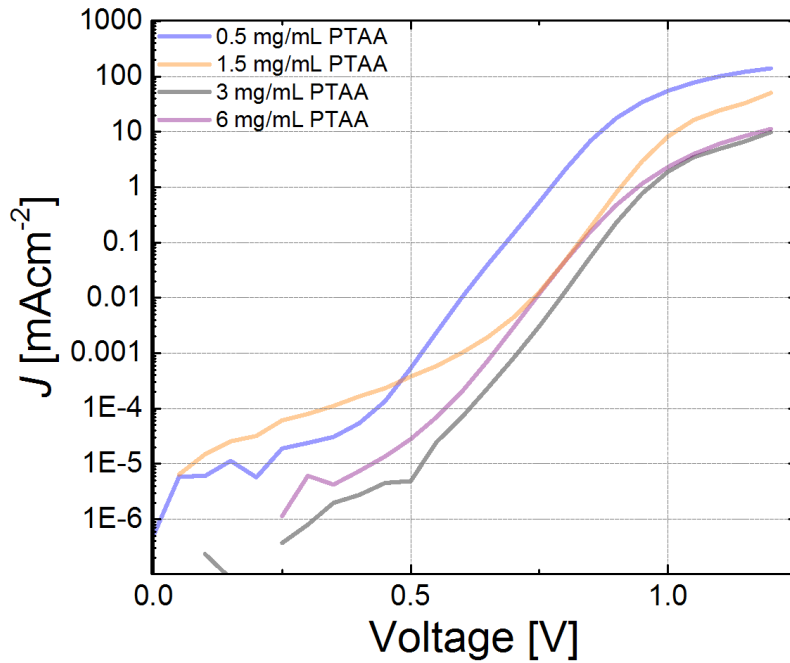


**Figure S2.** (a, b) Atomic force profiles of a scratch on as cast glass/PTAA films fabricated

from a 10 mg/mL PTAA solution (a) and 3 mg/mL (b) in toluene. PTAA thicknesses of 34.5 nm and 13.5 nm were obtained as indicated by the blue lines from the 10 mg/mL and 3 mg/mL solutions, respectively. (c, d) Atomic force profiles of a scratch on glass/PTAA films which were exposed to the perovskite solvent (DMF:DMSO 4:1) fabricated from the 10 mg/mL PTAA (c) and 3 mg/mL (d) solution. PTAA thicknesses of 34.4 nm and 12.1 nm were obtained as indicated by the blue lines. The insets show microscope images respectively.



**Supplementary Figure 3S.** (a) Averaged JV characteristics of triple cation perovskite solar cells with varying C60 electron transport layer thicknesses (based on 6 cells for each thickness). Above a C<sub>60</sub> thickness of 14 nm we found a relatively constant fill factor and performance, which indicates that the charge transport through the C<sub>60</sub> is not limiting the performance. We assign this to the significantly larger mobility of C<sub>60</sub> compared to PTAA.



**Supplementary Figure 4S.** Dark current density vs. voltage curves of solar cells with varying PTAA concentration, record in forward direction at 10 mV/s. We note that the dark current depends significantly on the stabilization time, and it usually decreases with increasing stabilization time.

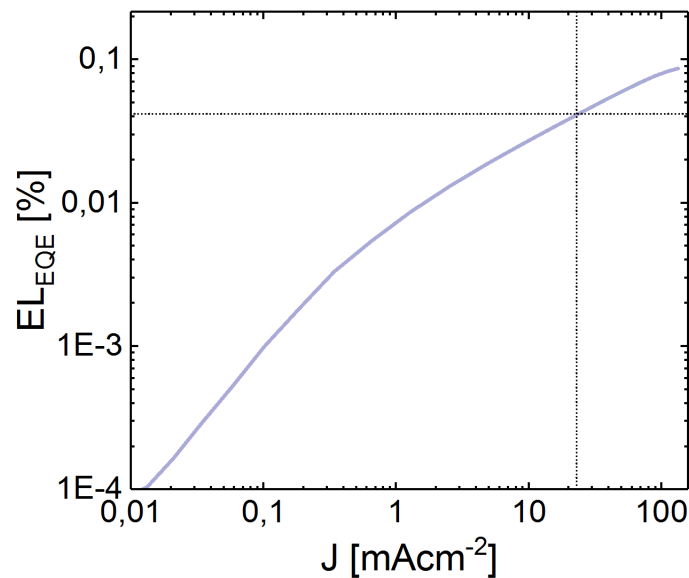
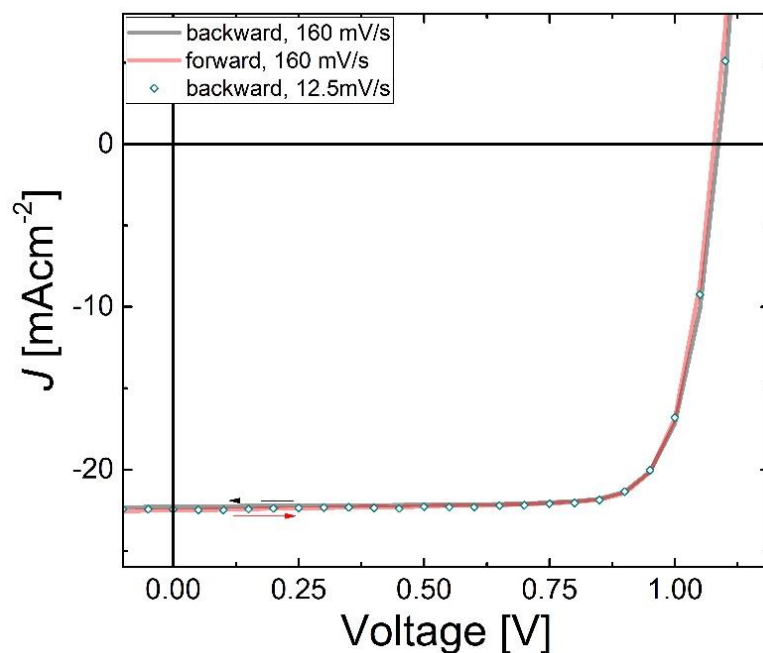
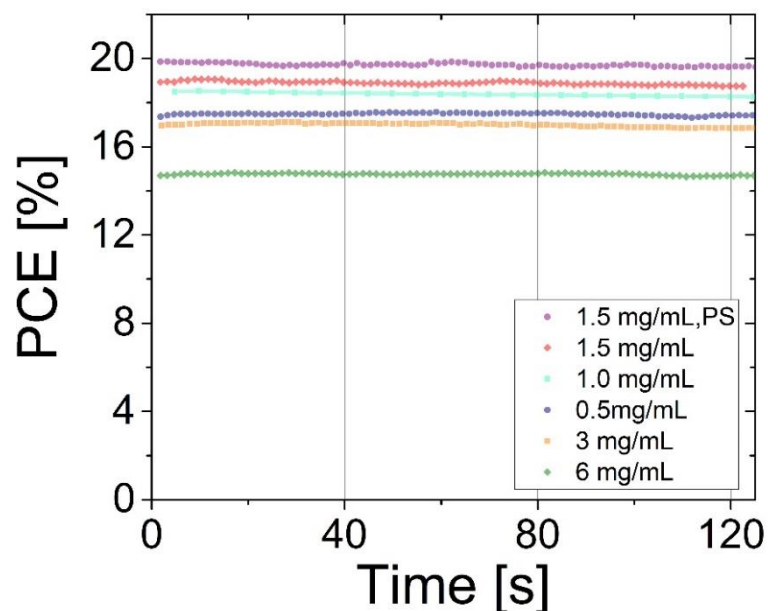


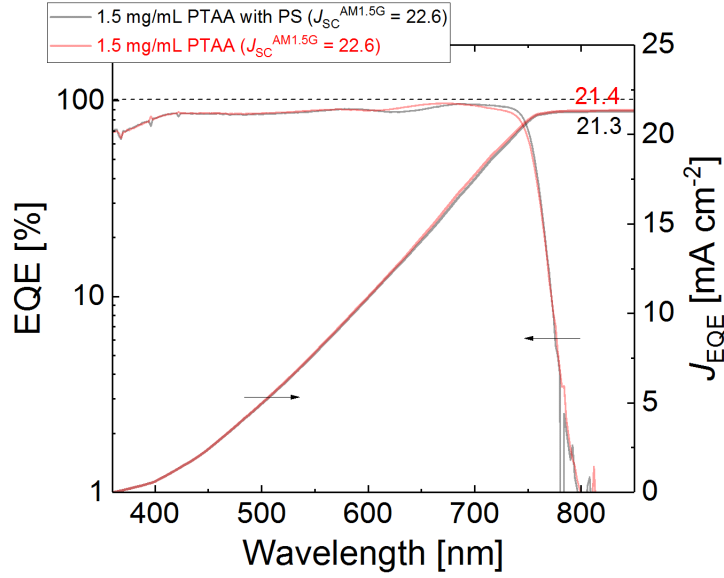
**Figure 5S.** Electroluminescence yield of perovskite cells fabricated with the optimum concentration of PTAA of 1.5 mg/m versus the (with applied voltage) injected dark current density. The short-circuit current density is marked at which an EL yield of  $\sim 4 \times 10^{-4}$  is obtained.



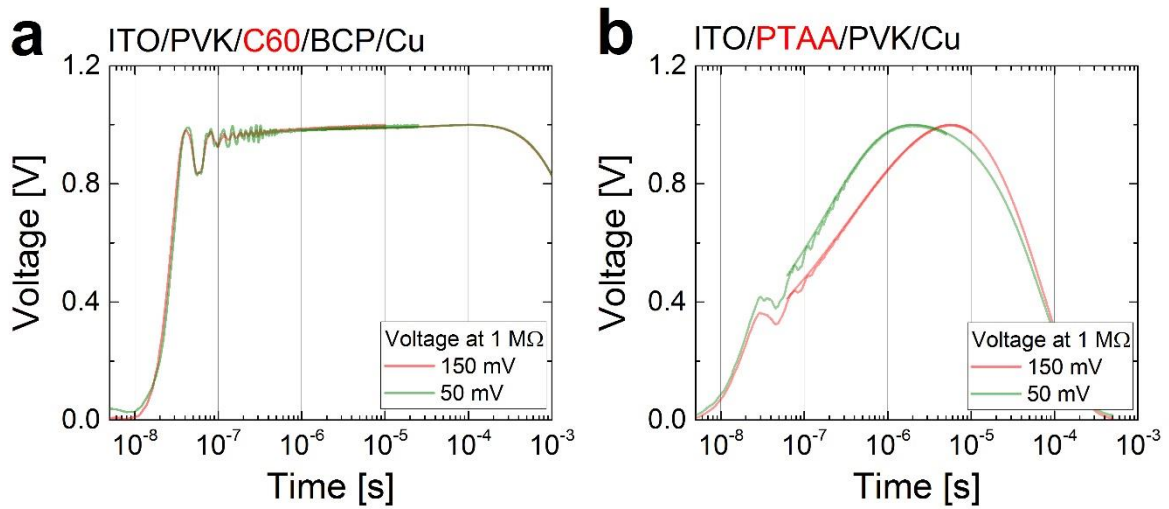
**Supplementary Figure 6S.** Representative current-density versus voltage characteristics of perovskite cells fabricated with the optimum concentration of PTAA of 1.5 mg/mL. No hysteresis is observed, which is typical for all studied cells. The JV-curves are also independent on the scan-speed as shown here for  $160 \text{ mV s}^{-1}$  (lines) or  $12.5 \text{ mV s}^{-1}$  (points).



**Supplementary Figure 7S.** The stabilized maximum power output under AM1.5G illumination of representative cells with varying PTAA concentrations.

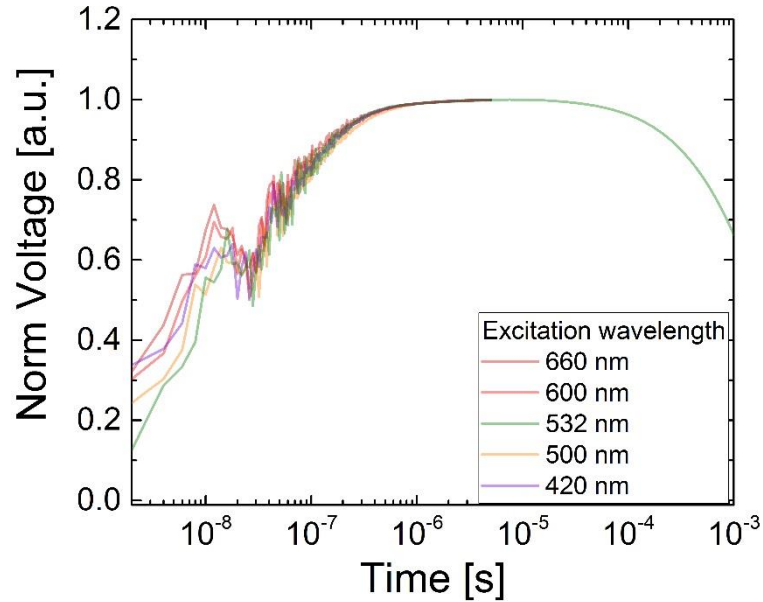


**Supplementary Figure 8S.** External quantum efficiency (EQE) spectra of a perovskite solar cell fabricated from a PTAA concentration of 1.5 mg/mL w/o. polystyrene (record configuration). The integral of the EQE and the AM1.5G solar spectrum yields a short-circuit current density of 21.3 and 21.4 mAcm<sup>-2</sup>, which matches the current density from the JV-curve under simulated AM1.5G within 5%.

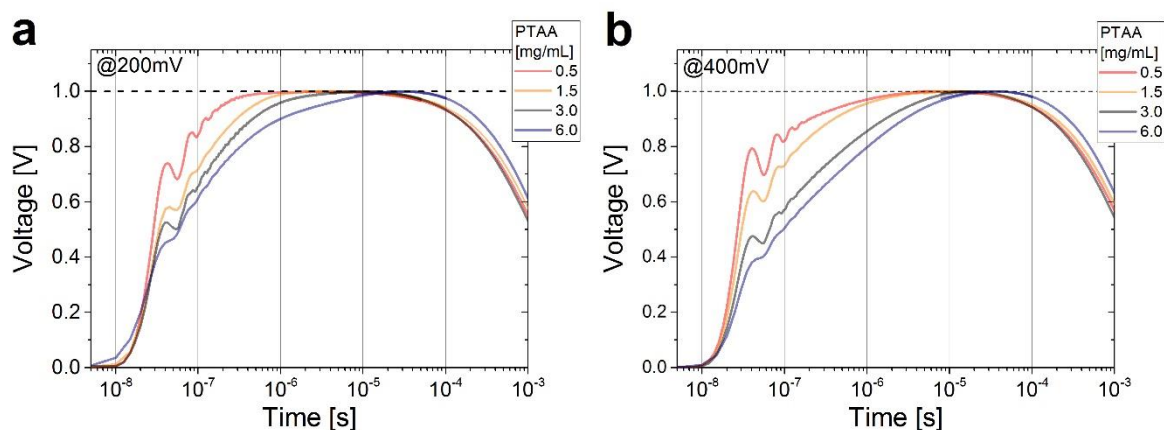


**Supplementary Figure 9S.** Normalized Integral Time of Flight transients of perovskite cells (a) without the PTAA HTL but with a 20 nm thick C<sub>60</sub> ETL and (b) without the C<sub>60</sub> ETL but with a PTAA layer coated from a 1.5 mg/mL solution. The rapid saturation of the photovoltage of the device without the PTAA proves the fast transit of charges through the perovskite and C<sub>60</sub> layer (~ 20 nm) on time-scales shorter than the response limit of our setup (tens of ns). In contrast, in at device without the C<sub>60</sub> (and BCP) layer, longer extraction times are observed

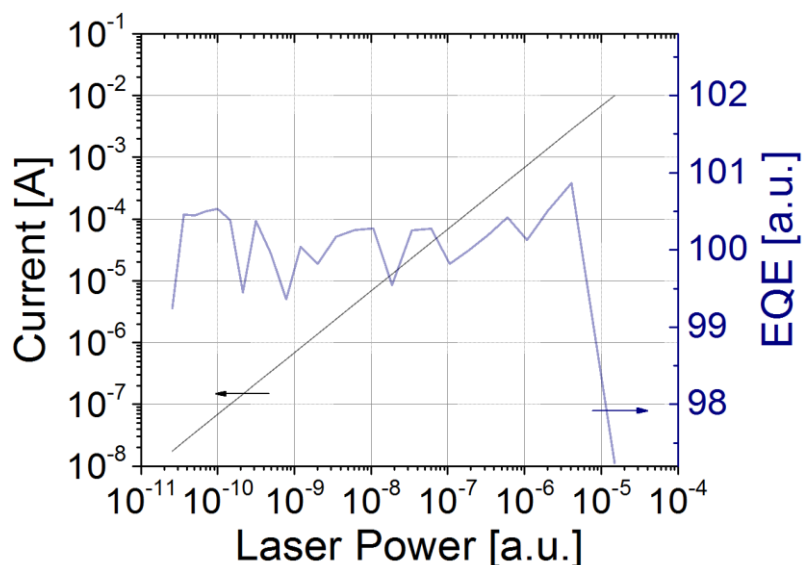
(on similar time scales as observed for the complete devices) due to the relatively slow transit of charges through the PTAA (~ 10 nm).



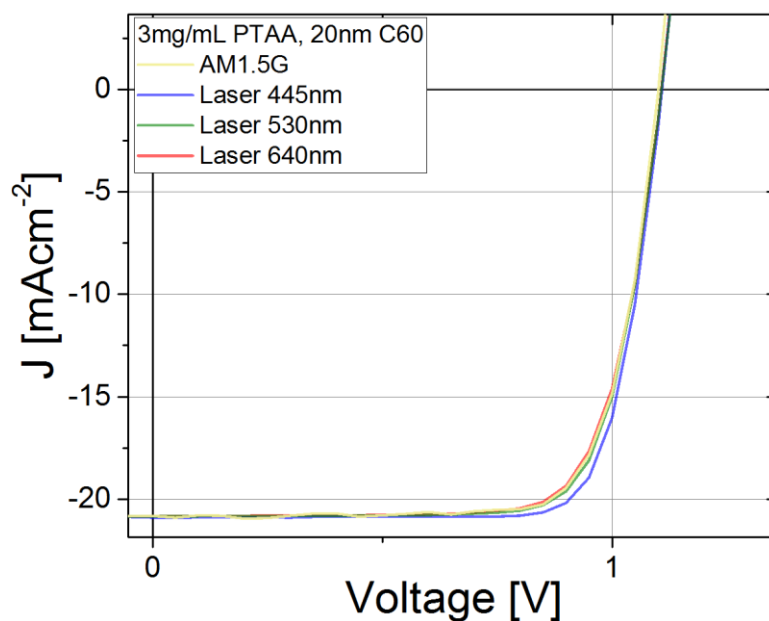
**Supplementary Figure 10S.** Normalized transient photovoltage signals recorded on a device fabricated from 1.5 mg/mL PTAA at a load resistance of 1 M $\Omega$  at different excitation wavelengths. The fluence at each wavelength was adjusted to produce the same photovoltage ( $U$ ) of 150 mV and same amount of charge in the device ( $CU$ , where  $C$  is the capacitance). The wavelength independent carrier arrival time shows that the carrier distribution profile in the perovskite does not influence the result. This also indicates that the travel time of photocarriers to the transport layers is not limiting the transport due to the significantly higher mobility in the perovskite compared to the organic layers. We note that the transit time remains independent on the excitation wavelength also at higher fluences and photovoltages.



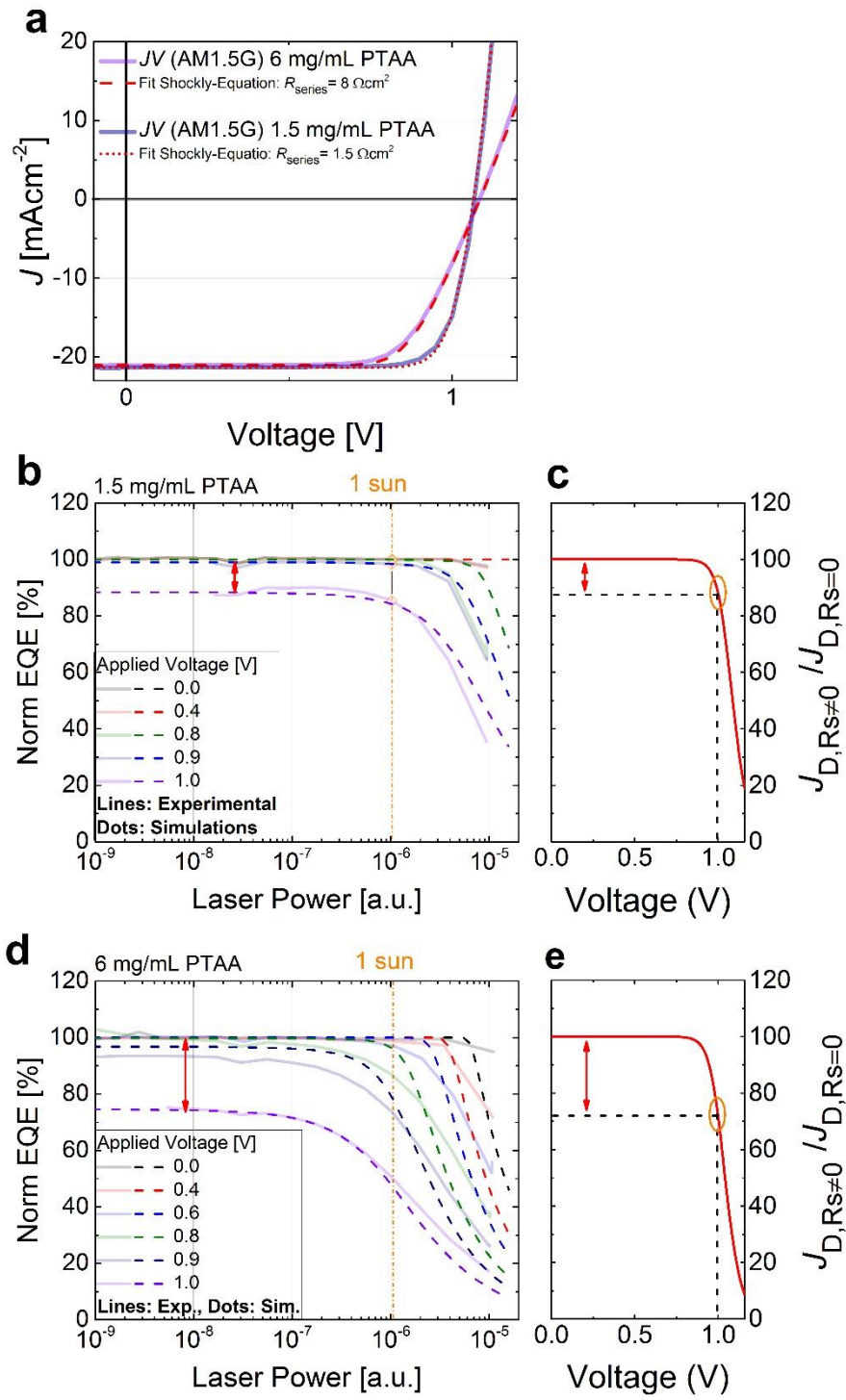
**Supplementary Figure 11S.** Normalized transient signals for the perovskite devices with different hole transport layer thicknesses recorded at a load resistance of  $1\text{ M}\Omega$  producing a photovoltage of (a) 200 mV (and a fluence of approximately  $60\text{ nJcm}^{-2}$ ) and (b) 400 mV (approximately  $140\text{ nJcm}^{-2}$ ). The graph reveals a fluence dependence of the charge carrier transit times, although the trend among the devices – the thinner the HTL, the shorter the transit time, and the higher the FF – remains unchanged.



**Supplementary Figure 12S.** Original intensity dependent photocurrent (IPC) data in steady-state measured on a device from 1.5 mg/mL PTAA at 0 V demonstrating the high precision of our setup. The variation of the EQE is as low as 1% across 6 orders of magnitude in light intensity.



**Supplementary Figure 13S.** *Excitation wavelength dependent (JV) characteristic measured on a device from 3 mg/mL PTAA. The laser power at each wavelength was adjusted to produce the short circuit current under AM1.5G illumination (1 sun equivalent power). The graph shows small variations in the JVs depending on the excitation wavelengths, however, this does not prevent general conclusions about the recombination order along the JV-curve under AM1.5G illumination.*



**Supplementary Figure 14S.** Intensity dependent photocurrent simulations. In order to model the experimental data of **Figure 5**, and in particular the limiting first-order losses close to the  $V_{OC}$ , we numerically solved the Shockley-equation  $J \sim -J_G + J_{G,0} \exp\left(\frac{q(V-JR_s)}{n_{ID}k_B T}\right)$  considering the impact of a variable series ( $R_s$ ). We note that the shunt resistance has no impact on the

intensity dependent EQE curves, as the EQE was obtained from the ratio of the photocurrent (light minus dark current) and the light intensity. **(a)** Using the measured ideality factor (**Figure 3a**), we fitted the IV-curve by using the series resistance as a fit parameter (specified in the label.). **(b, d)** Finally, we simulated the intensity dependent photocurrent data (dashed lines) using the obtained values for the series resistance and ideality factor. Notably, the features of the first order and higher order losses can be perfectly reproduced. **(c, e)** show that the magnitude of the limiting first-order recombination losses corresponds approximately to the ratio of the dark current with ( $J_D$ ) and without the series resistance ( $J_{D,RS=0}$ ) being present. This is in accordance with an analytical approximation, based on the Shockley equation, which gives in the limit of small generation currents ( $J_G$ ):  $EQE(V) \sim 1 - qJ_D(V)R_s / (n_{ID}k_B T) \sim \frac{J_D(V)}{J_{D,RS=0}(V)}$ .

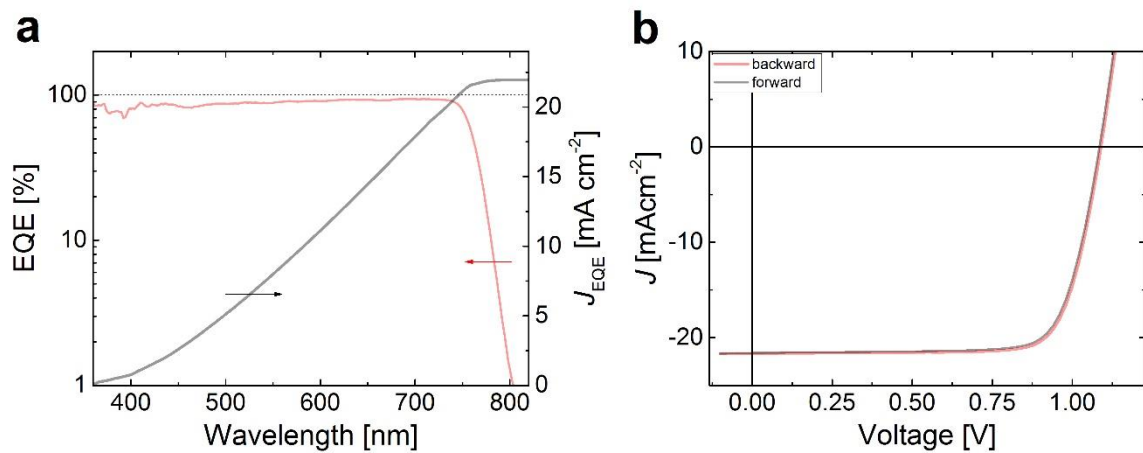


**Figure 15S.** **(a)** External quantum efficiency (EQE) spectra of champion  $1\text{cm}^2$  triple cation perovskite solar cells. The integral of the EQE and the AM1.5G solar spectrum yields a short-circuit current density of  $21.9\text{ mAcm}^{-2}$ , which matches the current density from the JV-curve under simulated AM1.5G within  $\pm 5\%$ . **(b)** Current-density versus voltage characteristics of the  $1\text{cm}^2$  triple cation perovskite solar cell measured unencapsulated in air, 1 month after fabrication under AM1.5G illumination at the Institut für Silizium Photovoltaik, Helmholtz-Zentrum Berlin für Energie und Materialien, Berlin-Adlershof at a scan rate of  $100\text{ mV/s}$ . This measurement yielded a PCE of  $18.4\%$ .

## Supplementary Note 1

Using the Shockley equation we can derive the conditions under which first- and higher-order recombination losses with respect to the light intensity are induced through the presence of a series resistance.

In the Shockley-model, the light current density is given as

$$J_L = J_R - J_G = J_{G,0} \exp\left(\frac{eV_i}{n_{ID}k_B T}\right) - J_G = J_{G,0} \exp\left(\frac{V_i}{n_{ID}V_{th}}\right) - J_G = J_{G,0} \exp\left(\frac{V_{appl} - J_L R_s}{n_{ID}V_{th}}\right) - J_G,$$

where  $J_R, J_G, J_{G,0}$  are the recombination, generation and dark generation current densities;  $V_i, V_{th}, V_{appl}$  the internal, thermal and applied voltages;  $n_{ID}$  the ideality factor,  $k_B, T$  the Boltzmann constant and the temperature, and  $R_s$  the series resistance.

Similar to that, the dark current density is given by

$$J_D = J_R(V_i) = J_{G,0} \exp\left(\frac{V_{appl} - J_D R_s}{n_{ID}V_{th}}\right) = J_{G,0} \exp\left(\frac{V_{appl}}{n_{ID}V_{th}}\right) \exp\left(\frac{-J_D R_s}{n_{ID}V_{th}}\right) = J_{D,R_s=0} \exp\left(\frac{-J_D R_s}{n_{ID}V_{th}}\right)$$

where  $J_{D,R_s=0}$  is the dark current at  $V_{appl}$  if no series resistance would be present.

Finally, the photocurrent density is defined as  $J_{ph} = J_L - J_D$ , with  $\text{EQE} = -\frac{J_{ph}}{J_G}$

Thus, we can write for the current density under illumination

$$\begin{aligned} J_L &= J_{G,0} \exp\left(\frac{V_{appl} - J_L R_s}{n_{ID}V_{th}}\right) - J_G = J_{G,0} \exp\left(\frac{V_{appl} - (J_{ph} + J_D) R_s}{n_{ID}V_{th}}\right) - J_G \\ &= J_{G,0} \exp\left(\frac{V_{appl} - (-\text{EQE} J_G + J_D) R_s}{n_{ID}V_{th}}\right) - J_G = \\ &= J_{G,0} \exp\left(\frac{V_{appl} - J_D R_s + \text{EQE} J_G R_s}{n_{ID}V_{th}}\right) - J_G = J_D \exp\left(\frac{\text{EQE} J_G R_s}{n_{ID}V_{th}}\right) - J_G \end{aligned}$$

and for the photocurrent density:

$$J_{ph} = J_L - J_D = J_D \exp\left(\frac{\text{EQE} J_G R_s}{n_{ID}V_{th}}\right) - J_G - J_D = J_D \left[ \exp\left(\frac{\text{EQE} J_G R_s}{n_{ID}V_{th}}\right) - 1 \right] - J_G$$

This leads to the following result for the EQE:

$$\text{EQE} = -\frac{J_{\text{ph}}}{J_{\text{G}}} = -\frac{-J_{\text{D}} \left[ \exp\left(\frac{\text{EQE} J_{\text{G}} R_{\text{s}}}{n_{\text{ID}} V_{\text{th}}}\right) - 1 \right] + J_{\text{G}}}{J_{\text{G}}} = 1 - \frac{J_{\text{D}}}{J_{\text{G}}} \left[ \exp\left(\frac{\text{EQE} J_{\text{G}} R_{\text{s}}}{n_{\text{ID}} V_{\text{th}}}\right) - 1 \right]$$

Using  $\exp(x) = 1 + x + \frac{1}{2}x^2 + \dots$ , we can approximate EQE by

$$\begin{aligned} \text{EQE} &= 1 - \frac{J_{\text{D}}}{J_{\text{G}}} \left[ \frac{\text{EQE} J_{\text{G}} R_{\text{s}}}{n_{\text{ID}} V_{\text{th}}} + \frac{(\text{EQE} J_{\text{G}} R_{\text{s}})^2}{2(n_{\text{ID}} V_{\text{th}})^2} + \dots \right] = 1 - \frac{\text{EQE} J_{\text{D}} R_{\text{s}}}{n_{\text{ID}} V_{\text{th}}} - \frac{1}{2} \frac{J_{\text{D}} J_{\text{G}} (\text{EQE} R_{\text{s}})^2}{(n_{\text{ID}} V_{\text{th}})^2} + \dots \\ &= 1 - \frac{\text{EQE} J_{\text{D}} R_{\text{s}}}{n_{\text{ID}} V_{\text{th}}} - \frac{1}{2} \frac{J_{\text{D}} J_{\text{ph}} \text{EQE} (R_{\text{s}})^2}{(n_{\text{ID}} V_{\text{th}})^2} \\ \rightarrow 1 &= \text{EQE} + \frac{\text{EQE} J_{\text{D}} R_{\text{s}}}{n_{\text{ID}} V_{\text{th}}} + \frac{1}{2} \frac{J_{\text{D}} J_{\text{ph}} \text{EQE} (R_{\text{s}})^2}{(n_{\text{ID}} V_{\text{th}})^2} = \text{EQE} \left( 1 + \frac{J_{\text{D}} R_{\text{s}}}{n_{\text{ID}} V_{\text{th}}} + \frac{1}{2} \frac{J_{\text{D}} J_{\text{ph}} (R_{\text{s}})^2}{(n_{\text{ID}} V_{\text{th}})^2} \right) \end{aligned}$$

$$\rightarrow \text{EQE} = \frac{1}{1 + \frac{J_{\text{D}} R_{\text{s}}}{n_{\text{ID}} V_{\text{th}}} + \frac{1}{2} \frac{J_{\text{D}} J_{\text{ph}} (R_{\text{s}})^2}{(n_{\text{ID}} V_{\text{th}})^2} + \dots}$$

Thus higher-order recombination can be neglected if  $\frac{J_{\text{D}} J_{\text{ph}} (R_{\text{s}})^2}{(n_{\text{ID}} V_{\text{th}})^2} \ll 1$ . In first order approximation this gives

$$\text{EQE} = \frac{1}{1 + \frac{J_{\text{D}} R_{\text{s}}}{n_{\text{ID}} V_{\text{th}}}}$$

For small  $\frac{J_{\text{D}} R_{\text{s}}}{n_{\text{ID}} V_{\text{th}}} \ll 1$  this simplifies to

$$\text{EQE} \cong 1 - \frac{J_{\text{D}} R_{\text{s}}}{n_{\text{ID}} V_{\text{th}}}$$

$$\text{Using } J_{\text{D}} = J_{\text{D}, \text{Rs}=0} \exp\left(\frac{-J_{\text{D}} R_{\text{s}}}{n_{\text{ID}} V_{\text{th}}}\right) \cong J_{\text{D}, \text{Rs}=0} \left(1 - \frac{J_{\text{D}} R_{\text{s}}}{n_{\text{ID}} V_{\text{th}}}\right)$$

we can also approximate the first order EQE losses with

$$\text{EQE} \cong 1 - \frac{J_{\text{D}} R_{\text{s}}}{n_{\text{ID}} V_{\text{th}}} \cong \frac{J_{\text{D}}}{J_{\text{D}, \text{Rs}=0}}$$

i.e. the ratio of the dark current and the dark current without series resistance, as shown in **Figure 14S**.